



OPEN

High magnetic field phase diagram in
electron-doped manganitesChengliang Lu¹, Ni Hu², Ming Yang¹, Shuangcheng Xia¹, Haowen Wang¹, Junfeng Wang¹, Zhengcai Xia¹
& Jun-Ming Liu³SUBJECT AREAS:
MAGNETIC PROPERTIES
AND MATERIALS
APPLIED PHYSICSReceived
7 November 2013Accepted
10 April 2014Published
9 May 2014Correspondence and
requests for materials
should be addressed to
C.L.L. (cllu@mail.hust.
edu.cn) or J.M.L.
(liujm@nju.edu.cn)¹Department of Physics & Wuhan National High Magnetic Field Center, Huazhong University of Science and Technology, Wuhan 430074, China, ²Department of Physics, Hubei University of Technology, Wuhan 430068, China, ³Laboratory of Solid State Microstructures, Nanjing University, Nanjing 210093, China and Institute for Quantum Materials, Hubei Polytechnic University, Huangshi 435000, China.

We report the charge-order to ferromagnetic phase transition induced by pulsed high magnetic field and impurity doping effects in manganites $\text{La}_{0.4}\text{Ca}_{0.6}(\text{Mn}_{1-y}\text{Cr}_y)\text{O}_3$ ($0 \leq y \leq 0.2$). Significant charge-order suppression and ferromagnetic tendency upon the Cr^{3+} -doping are evidenced, and three different ground states are identified, namely the charge-order state, the phase separated state, and the spin-glass like state. Phase diagram in the H - y plane at 4.2 K is determined by the high magnetic field study, in which the charge-order and ferromagnetic phase boundary is clearly figured out. The critical magnetic field for melting the charge-order phase of $\text{La}_{0.4}\text{Ca}_{0.6}\text{MnO}_3$ is revealed to reach up to 46 T at 4.2 K. Interestingly, distinct responses of the three states to the high magnetic field are observed, indicating the special physics regarding the charge order melting process in each state. The mechanism of the doping induced charge-order suppression and ferromagnetism promotion can be understood by the competition between the antiferromagnetic interaction of Cr-Mn and local enhancement of electron hopping by Cr^{3+} .

Perovskite manganites $\text{RE}_{1-x}\text{AE}_x\text{MnO}_3$, where RE is the rare-earth element and AE the divalent alkaline-earth element, have attracted considerable attention due to the presence of multiple competing phases with essentially distinct physical properties but proximate free energies^{1,2}. The delicate balance among the diverse phases can be easily tilted through “weak” external or internal perturbations, and thus dramatic variation of the physical properties can be achieved. One of the typical examples is the magnetic field driven charge-order (CO) to ferromagnetic (FM) phase transition, which is accompanied by an insulator-metal transition and tremendous reduction in resistivity—the *colossal magnetoresistance* (CMR)^{3–5}.

The CO-FM phase transition is crucial for understanding the competition among various exchange interactions not only in CMR manganites but also in other magnetic transition metal oxides, and indeed attractive for potential applications due to the concurrent huge change in resistivity. For manganites, most of earlier investigations were focusing on hole-doped or half-doped CO systems ($x \leq 0.5$), and the phase boundary between the CO and FM phases in these materials was well figured out^{2,6}. According to the phase diagram of $\text{Pr}_{1-x}\text{Ca}_x\text{MnO}_3$, the critical field of the CO-FM transition increases dramatically with increasing x from 0.3 to 0.5⁶, suggesting a distinct enhancement of the CO-state-stability due to the reduction of e_g electron density. This relation is reasonably well understood since higher e_g electron density always favors the double exchange FM interaction which competes with the charge-ordering. In this sense, more stable CO state in electron-doped region $x > 0.5$ in the phase diagram would be expected upon further decreasing the e_g electron density.

In fact, the CO-FM phase transition in electron-doped CO manganites ($x > 0.5$) was less studied, while it is currently receiving more and more interests since the electron doping is remarkably asymmetric from the hole doping in terms of electronic structure, magnetism, and transport behaviors^{7–11}. In $\text{Sm}_{1-x}\text{Ca}_x\text{MnO}_3$ ($0.5 < x \leq 0.85$)¹², the CO melting magnetic field was revealed to decrease monotonously with increasing x , while the e_g electron density decreases simultaneously. Recently, although the CO state is very robust in $\text{La}_{1-x}\text{Ca}_x\text{MnO}_3$ ($0.5 < x \leq 0.87$)^{13,14}, exceptional CO breaking and ferromagnetism upon size reduction (down to nano-scale) or impurity doping was broadly reported^{15–20}. Moreover, photo-induced CO melting was observed in $\text{La}_{0.42}\text{Ca}_{0.58}\text{MnO}_3$, and the threshold fluence for melting the CO phase was revealed to be significantly lower than that for hole-doped $\text{La}_{1/4}\text{Pr}_{3/8}\text{Ca}_{3/8}\text{MnO}_3$ ^{21,22}, which seems inconsistent with the fact that an electron-doped material has a much more stable CO state^{13,23}. These works revealed interesting CO suppression and FM

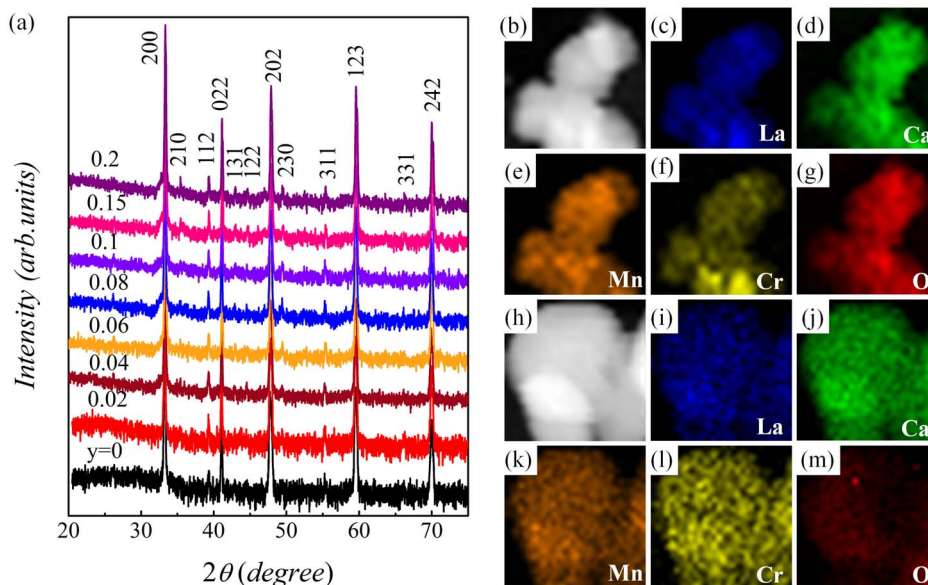


Figure 1 | (a) X-Ray diffraction θ - 2θ spectra at room temperature for a series of samples $\text{La}_{0.4}\text{Ca}_{0.6}(\text{Mn}_{1-y}\text{Cr}_y)\text{O}_3$ ($0 \leq y \leq 0.2$). High angle annular dark field scanning transmission electron microscopy for samples (b): $y = 0.1$ and (h): $y = 0.2$, and corresponding elemental mappings by using energy dispersive X-ray spectrometer of La, Ca, Mn, Cr, and O for samples (c) – (g): $y = 0.1$ and (i) – (m): $y = 0.2$.

generation in the impurity-doped or nano-scaled CO manganites $\text{La}_{1-x}\text{Ca}_x\text{MnO}_3$ ($0.5 < x \leq 0.87$), while the CO and FM phase boundary in these materials is not revealed until now.

On the other hand, the magnetic field induced CO melting process for phase separated (PS) state²⁴, in which the CO and FM phases coexist and compete with each other, was found to be very different from that of the pure CO state in half-doped CO manganites⁶. It originates from an additional elastic energy arising at the CO and FM domain walls in the PS manganite, which prefers to block the magnetic field driven CO-FM phase transition. Following this line, it would be of interest to investigate the magnetic response of the CO phase within a PS state or spin-glass (SG) like state caused by the competition among diverse exchange interactions²⁵. The consideration is that the possible magnetic field induced CO melting in these states would be further challenged by the spin freezing, in addition to the elastic energy at the CO/FM domain walls and free energy barriers between CO and FM phases.

In present work, $\text{La}_{0.4}\text{Ca}_{0.6}\text{MnO}_3$ is selected as the prototype CO manganite to study the CO-FM phase transition since it has nearly the highest CO phase transition temperature ($T_{\text{CO}} \sim 260$ K). The roughly pre-estimated CO melting field in $\text{La}_{0.4}\text{Ca}_{0.6}\text{MnO}_3$ should be higher than 20 T, supported by the fact that the value in $\text{La}_{0.5}\text{Ca}_{0.5}\text{MnO}_3$ is already as high as $H = 20$ T²⁶, and the CO state becomes even more stable upon increasing the Ca^{2+} content to 0.6^{13,14}. In this sense, pulsed high magnetic field (up to 55 T) is used to make the present investigation feasible. Besides the pulsed high magnetic field, Cr^{3+} -doping is utilized simultaneously to study the CO-FM phase transition in $\text{La}_{0.4}\text{Ca}_{0.6}\text{MnO}_3$. The consideration for choosing Cr^{3+} as the doping species is threefold. First, the Cr^{3+} charge valence was confirmed to be stable in doped CO manganites²⁷, which would simplify the underlying physics. Second, Cr^{3+} -doping was revealed to be effective in mediating the CO suppression and FM promotion in CO manganites, because it allows lattice defect and magnetic coupling with Mn simultaneously^{28–30}, which would weaken the CO state in $\text{La}_{0.4}\text{Ca}_{0.6}\text{MnO}_3$ and thus facilitate our investigation. Third, various ground states, such as pure CO state, PS state, and SG-like state, are expected through Cr^{3+} -doping based on the aforementioned reasons, providing an opportunity to systematically investigate the evolution of the CO-FM phase transition as the ground state varies from the pure CO state to the SG one. Our

results reveal significant CO suppression and FM tendency upon the Cr^{3+} -doping at Mn-site in $\text{La}_{0.4}\text{Ca}_{0.6}\text{MnO}_3$. Three different states, including the CO state, the PS state, and the SG-like state are identified. High magnetic field study reveals an interesting CO-FM phase transition, and the three states show distinct responses to the high magnetic field.

Results

In Fig. 1(a), we present the measured X-ray diffraction (XRD) θ - 2θ patterns at room temperature for all samples. Pure orthorhombic crystalline structure with space group $Pnma$ can be identified for all samples. The diffraction peak positions are identical for all samples, indicating no evident change in lattice parameters upon the Cr^{3+} -doping. This is consistent with the similar ionic radius between Cr^{3+} and Mn^{3+} . Furthermore, we show in Fig. 1(b)–(m) the elemental mappings using the energy-dispersive X-ray spectrometer (EDS), which suggests the homogeneous distributions of La, Ca, Mn, Cr, and O. To investigate the Cr^{3+} -doping induced modulation on physical properties, we subsequently measured the magnetization of the samples under various conditions.

As we expect, the CO and antiferromagnetic (AFM) phase transitions for the sample with $y = 0$ ($\text{La}_{0.4}\text{Ca}_{0.6}\text{MnO}_3$) arise at $T_{\text{CO}} = 260$ K and $T_{\text{N}} = 143$ K, respectively, shown in Fig. 2(a). Both phase transitions well match the data in literature¹, indicating good quality of our samples. Upon the Cr^{3+} -doping, the $M(T)$ curves present clear downward shift in both T_{CO} and T_{N} , implying strong suppression of the CO/AFM state. With $y > 0.06$, the CO phase transition becomes ambiguous, but the broad magnetic upturn around 275 K (indicated by green arrows in Fig. 2) related to the initiation of the CO phase can still be observed. This feature suggests a crossover from long range CO phase to short range one happening at $y \sim 0.06$. For the sample with $y = 0.2$, both T_{N} and T_{CO} disappear but instead, a cusp-like peak arises at $T_{\text{f}} \sim 68$ K in the ZFC case, and subsequently large bifurcation emerges between the FC and ZFC curves. These features are typical characteristics of a SG state²⁵, and hence lead us to argue a possible SG-like transition occurring at $T_{\text{f}} \sim 68$ K in the sample with $y = 0.2$. Additionally, the weak but sharp peak at $T_{\text{B}} \sim 40$ K in the ZFC case for the doped samples with $0.02 \leq y \leq 0.15$ is probably due to thermal blocking of finite AFM clusters considering their small magnetization ($M \sim 10^{-1}$ emu/g).

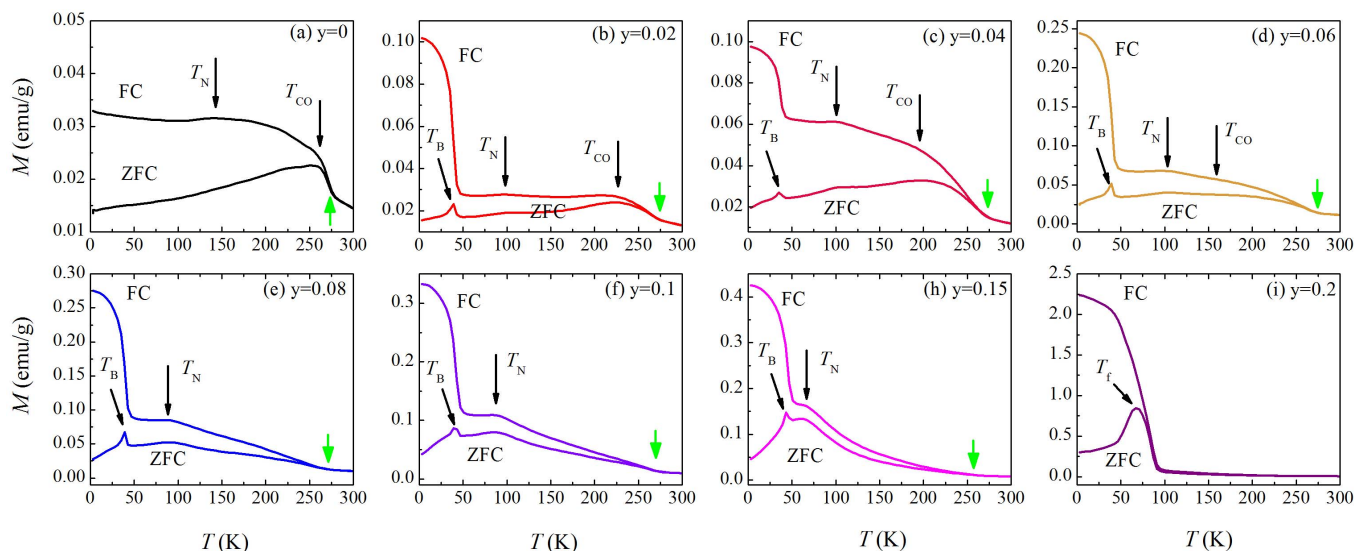


Figure 2 | Temperature profiles of magnetization at $H = 100$ Oe for all samples. The green arrow indicates the initiation of charge-ordering phase.

Actually, a similar phenomenon was reported in modestly doped CO manganite $\text{Pr}_{0.5}\text{Ca}_{0.5}(\text{Mn}_{0.975}\text{Al}_{0.025})\text{O}_3$ and was confirmed to be induced by the thermal blocking of nanoscale AFM clusters³².

To confirm the possible SG-like state in the sample with $y = 0.2$, ac magnetic susceptibility was performed and shown in Fig. 3(a). Significant downright frequency dispersion of the peaked χ' - T relation is identified, which characterizes the dynamic response of spins in the SG state. Here we use the critical slowing-down power law, assuming a true equilibrium phase transition with a divergence of relaxation time near the freezing point, to analyze spin dynamics of the SG state. We found a good scaling relation between $\varepsilon = (T_f/T_g - 1)$ and τ shown in Fig. 3(b), where T_f is the peak temperature measured at frequency f , T_g is the transition temperature in the low frequency limit, and τ is the observation time. According to the fitting with critical power law $\tau/\tau_0 = (T_f/T_g - 1)^{-z\nu}$ ^{33,34}, we obtained the critical exponents $z\nu = 4.4$, $T_g = 76.9$ K (consistent with T_f at low frequency), and $\tau_0 \sim 3.4 \times 10^{-9}$ s. The long spin flipping time τ_0 (\gg single spin flipping time 10^{-13} s) and relative small critical expo-

nent $z\nu$ suggest a cluster SG state in the sample $y = 0.2$ ^{33,34}, in which the Cr^{3+} -doping induced FM clusters are randomly oriented.

The H dependence of M measured at $T = 4$ K for all samples is shown in Fig. 4, which is useful to get more details on the phase evolution with the Cr^{3+} -doping. Evidently, very thin $M(H)$ hysteresis and small M can be seen for the samples with $y \leq 0.06$, confirming the robust long range CO/AFM state. For $y > 0.06$, the magnetic hysteresis becomes striking and M increases dramatically with y , which solidly suggests the emergence of a FM phase in the CO/AFM matrix. The remnant and maximum magnetization (M_r and M_m at $H = 5$ T) were derived from the $M(H)$ curves and plotted as a function of y in Fig. 5(a). Distinct increase of M_r and M_m ensues around $y = 0.06$, which marks the onset of FM phase and coincides with the crossover from long range CO phase to short range one evidenced by the $M(T)$ data. This fact indicates the essential role of the short range charge ordering in mediating the competition between FM and CO phases. Based on the $M(T)$ and $M(H)$ data, a T - y phase diagram is summarized in Fig. 5(b), in which the state evolution with y can be clearly seen. For $0 \leq y \leq 0.06$, the long range CO/AFM ground state is robust, while the uniform decrease in both T_{CO} and T_N signals the Cr^{3+} -doping induced suppression of the CO/

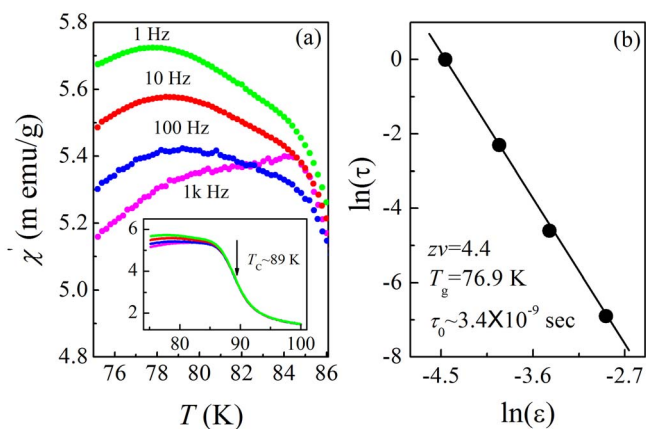


Figure 3 | (a) Measured ac susceptibility χ' as a function of T at $f = 1, 10, 100,$ and 1 k Hz for sample $y = 0.2$. The inset shows data in full measuring temperature range, in which the ferromagnetic phase transition is $T_C \sim 89$ K well matching the value of dc measurement. The difference in T_f obtained from the ac and dc data is due to the different measuring magnetic field. (b) dynamical scaling of the observation time τ with the reduced temperature $\varepsilon = (T_f/T_g - 1)$.

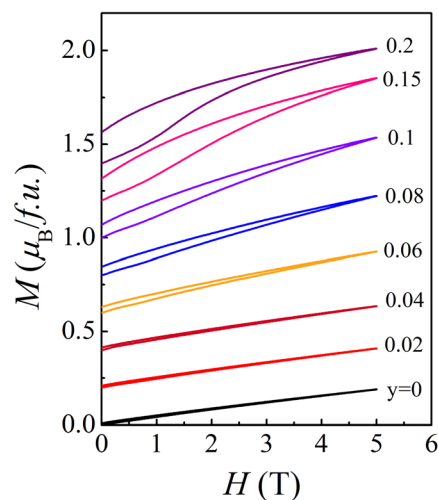


Figure 4 | Measured magnetization as a function of magnetic field at $T = 4$ K for all samples. Magnetization curves, except for the $y = 0$ data, are shifted upward ($0.2 \mu_B/f.u.$ in each shift) for clarity.

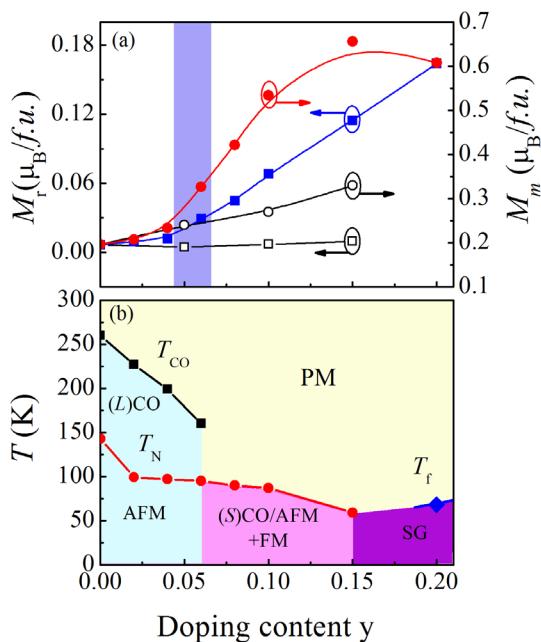


Figure 5 | (a) Remnant magnetization M_r (left axis) and maximum magnetization M_m at $H = 5$ T (right axis) as a function of doping content y . Solid circles and squares are the data from Cr^{3+} -doping samples, while open circles and squares are the data from Fe^{3+} -doping samples. The shadow region around $y = 0.06$ indicates the crossover from long range charge-order phase to a short range one due to the Cr^{3+} -doping. (b) Summarized T - y phase diagram, in which (L)CO means long range charge-order phase, and (S)CO means short range charge-order phase.

AFM phase. By the further increase of y from 0.06 to 0.15, the PS state arises, in which the short range CO/AFM orders and the FM phase coexist and compete with each other. As y reaches up to 0.2, a SG-like state arises due to the competition between FM and AFM interactions. In addition, the $M_m \sim 0.65 \mu_B/f.u.$ at $y = 0.15$ is $\sim 19\%$ of the expected moment $M \sim 3.4 \mu_B/f.u.$ in $\text{La}_{0.4}\text{Ca}_{0.6}\text{MnO}_3$, which is close to the percolation threshold value as predicted theoretically in the 3D percolation model³⁵. Therefore, it would be interesting to explore a possible CMR effect in the highly doped samples. However, insulating transport behaviors (shown in Fig. 6), even with applied magnetic field as high as $H = 10$ T, are revealed for samples with $y = 0.1, 0.15$, and 0.2 , pointing towards strong localization of electrons. Additional isothermal magneto-resistance data are plotted in Fig. 6(e). Clearly, just one to two orders of magnitude decrease in the resistivity can be seen as $H = 16$ T, suggesting the robust insulating state of the samples. In fact, we will see below that the critical field for inducing CO-FM phase transition is much higher than 10 T, which means that the applied magnetic field during the magneto-transport measurements is not high enough to generate a FM metallic state. Intriguingly, a positive MR can be seen in the sample with $y = 0.2$, which is probably due to the tunneling effect across insulating regions sandwiched by metallic phase³⁶. The transport behavior of the samples well follow the variable range hopping (VRH) model: $\rho = \rho_0 \exp[(T_0/T)^{1/4}]$, where ρ_0 is the pre-factor and T_0 is the characteristic temperature³⁷. It is consistent with the scenario of dominant CO-AFM state and strong localization of electrons in the samples.

The experimental results presented above indeed suggest three different states upon the Cr^{3+} -doping: the long range CO/AFM state, the PS state with coexisting short range CO/AFM and FM phases, and the SG-like state due to the competition between FM and AFM interactions. This provides an ideal avenue to systematically study the magnetic field driven CO-FM phase transitions between diverse ground states. The measured magnetization using pulsed high mag-

netic field at $T = 4.2$ K is shown in Fig. 7. Sharp CO-FM phase transitions and remarkable hysteresis in $M(H)$ curves are observed and particularly clear in the low Cr^{3+} -doping levels. The saturated magnetization is derived to be in the range of 3.1 to $3.3 \mu_B/f.u.$ for $y \leq 0.1$, and even smaller value appears in the samples with $y = 0.15$ and $y = 0.2$. The saturated moment of all the samples is lower than the expected value of $3.4 \mu_B/f.u.$ for Mn cation. Considering the very high sweeping rate of the pulsed magnetic field ($\sim 10^3$ T/second), a small part of the moments probably can't be well aligned by the field, thus inducing the relatively low saturated moment^{1,2}. This effect becomes more striking when the spin-glass state is involved, such as the case in the sample with $y = 0.2$. Considering the very robust CO state for the samples, spin tilting would happen in the resultant FM phase, which may be one of the reasons for the slightly smaller saturated magnetization of the FM state. An H - y phase diagram obtained from the high magnetic field data is shown in Fig. 7(b), where the critical fields (H_c) of the CO-FM phase transition are estimated from derivative of magnetization dM/dH (the inset of Fig. 7(b)).

Indeed, different evolving paths of H_c with y can be observed. For $0 \leq y \leq 0.06$ where the samples are in the CO/AFM ground state, H_c decreases rapidly with y corresponding to the dramatic decrease in T_{CO} . This can be easily understood by the competition between the Zeeman energy by external magnetic field and energy barrier between the CO and FM phases. Because of the Cr^{3+} -doping, the long range CO state is broken into short range orders, resulting in a smaller energy barrier between the CO and FM phases. In this sense, concurrent decreases of H_c and T_{CO} are reasonably expected upon increasing y . For $0.06 \leq y \leq 0.15$, where the samples have the PS ground state, the $H(y)$ curve becomes gentle and only slight variation in H_c can be seen. Based on the low magnetic field data, the FM phase emerges around $y = 0.06$ and its volume fraction shows distinct enhancement with further increasing of y , suggesting the continuous reduction of the CO and FM phase energy barrier. On the other side, as a consequence of the FM phase emergence, elastic energy related to the elastic strain arises at the interface of the CO and FM domain wall due to the different lattices of both phases, which tends to compete with the Zeeman energy and block the magnetic field driven CO-FM phase transition²⁴. Therefore, slight variation in H_c is evidenced, although the CO phase is largely suppressed within the doping range of $0.06 \leq y \leq 0.15$. In the sample with $y = 0.2$, the competition between FM and AFM interactions drives the SG-like state below T_f . Such spin freezing is a cooperative phenomenon and would further compete with the Zeeman energy besides the elastic energy and the barrier between the CO and FM phases. It is thus no magnetic field driven CO-FM phase transition and magnetic saturation can be observed in the sample with $y = 0.2$. Additionally, from the high field phase diagram, the Zeeman energy (E_1) driving the CO-FM phase transition can be derived to be of few meV. On the other hand, the free energy (E_2) of the CO state can be estimated from the T_{CO} , which is about tens of meV. Therefore, the energy of spin-charge coupling can be extrapolated to be $E = E_2 - E_1 \sim 10$ – 100 meV in these materials, which is responsible for the coexistence of AFM and CO phases in manganites. Here, we would like to mention that the sweeping rate of pulsed high magnetic field used in the present work is about five orders of magnitude higher than the quasi-static case, and thus it is not yet clear what variation is to be expected in these pulsed high magnetic field experiments with respect to those quasi-static field ones, which surely deserves further investigations.

Discussion

The mechanism of the Cr^{3+} -doping induced ferromagnetism can be discussed as the following. Generally, three straightforward effects can be induced by the Cr^{3+} -doping: i) disorder effect due to the lattice defects, which always frustrate the long range CO phase, ii) antiferromagnetic coupling between the Cr^{3+} and Mn cations³⁸, iii) substitution of Cr^{3+} for Mn^{3+} reduces the local e_g charge density, which

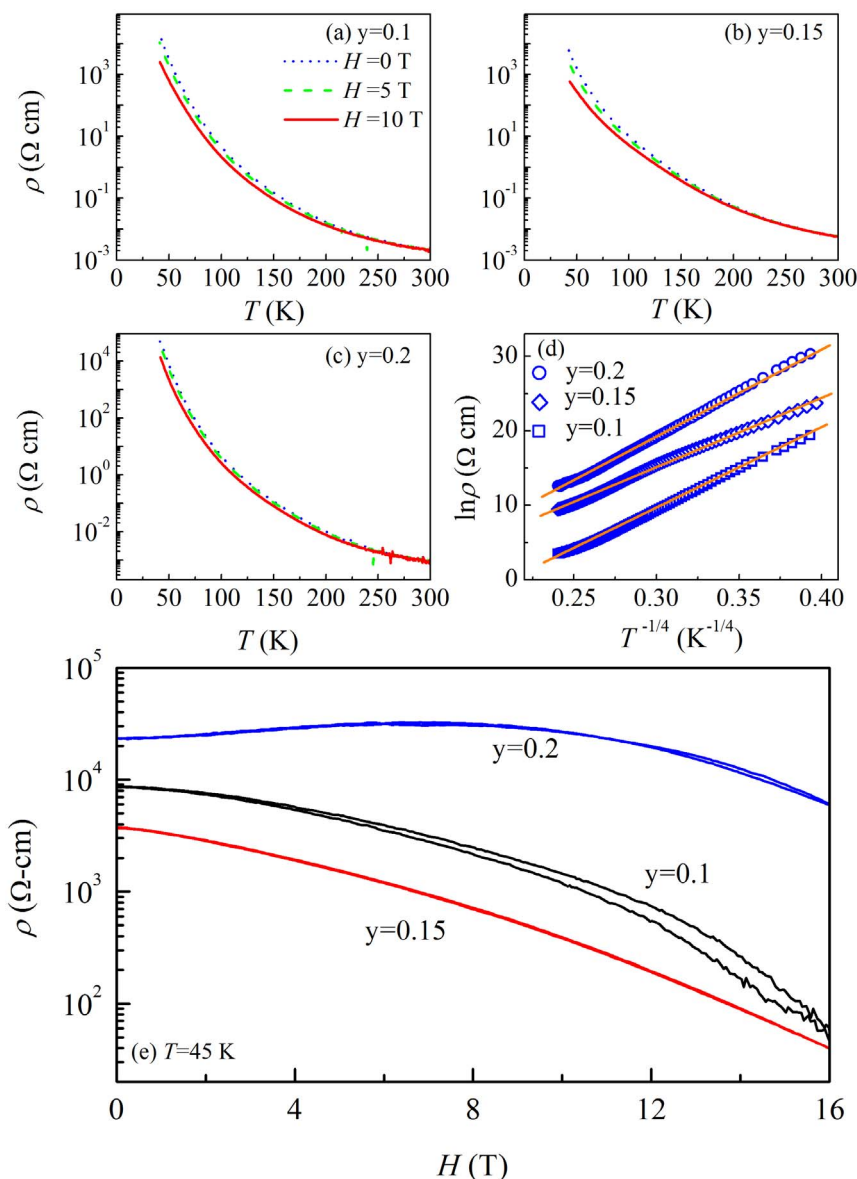


Figure 6 | Temperature profiles of resistivity at various applied magnetic fields for samples (a) $y = 0.1$; (b) $y = 0.15$; (c) $y = 0.2$. (d) Fitting of zero field resistivity ρ as a function of $T^{-1/4}$ using the variable range hopping model for the three samples. (e) Resistivity as a function of magnetic field for the three samples measured at $T = 45$ K.

stabilizes the AFM superexchange interaction. It is clear that the third factor has a negative contribution to the FM generation, and therefore we just need to consider the first two ones. The disorder effect is inevitable for the Mn-site doping, and plays an important role in the FM tendency in half-doped CO manganites. However, it was revealed that the disorder effect can not induce ferromagnetism although the CO/AFM state was dramatically suppressed in $\text{La}_{0.4}\text{Ca}_{0.6}\text{MnO}_3$ ³⁹. Hence, it is likely that the Cr-Mn AFM coupling is decisive for the FM phase promotion. In $\text{La}_{0.4}\text{Ca}_{0.6}\text{MnO}_3$, the AFM state is dominated by the CE-type order, which means a stacking of zigzag FM chains with inter-chain AFM coupling¹. Based on this picture, one may expect that the Cr^{3+} can be introduced into one zigzag chain without impacting the spin direction of the neighboring zigzag chains due to the Cr-Mn AFM interaction. On the contrary, within the Cr^{3+} -doped zigzag chain, the Mn moments will be reversed to maintain the Cr-Mn AFM interaction and inner-chain Mn-Mn FM coupling simultaneously, which gives rise to microscale FM clusters surrounding the Cr^{3+} ^{27,29}. However, such spin reversal would be vigorously competed by the inter-chain Mn-Mn AFM

interaction, and thus the FM clusters can only appear in case of largely weakened inter-chain AFM interaction, corresponding to the distinct enhancement of FM volume fraction of $0.06 \leq y \leq 0.15$ in the present work. In fact, submicrometric FM metallic clusters were reported in Cr^{3+} -doped $\text{Nd}_{1/2}\text{Ca}_{1/2}\text{MnO}_3$, supporting such kind of mechanism³⁰.

Furthermore, we also measured the $M(H)$ curves of Fe^{3+} -doped $\text{La}_{0.4}\text{Ca}_{0.6}\text{MnO}_3$ to make a comparison with the Cr^{3+} -doping effect, and the derived M_r and M_m are plotted in Fig. 5(a) (black open circles and squares). No FM phase can be detected in the Fe^{3+} -doping samples, although Fe^{3+} is closely analogous to Cr^{3+} , such as the same trivalence, close ionic radius to Mn^{3+} , and AFM coupling with Mn cations. Therefore, besides the AFM interaction of Cr-Mn, additional ingredient should be taken into account to understand the Cr^{3+} -doping induced CO suppression and FM promotion. We note that both of Fe^{3+} and Cr^{3+} are not Jahn-Teller (JT) active cations, which indicates an enhancement in local electron hopping strength due to the reduced JT effect by $\text{Fe}^{3+}/\text{Cr}^{3+}$ doping. However, different from the empty e_g state of Cr^{3+} (d^3), the $3d$ states of Fe^{3+} (d^5) with the same

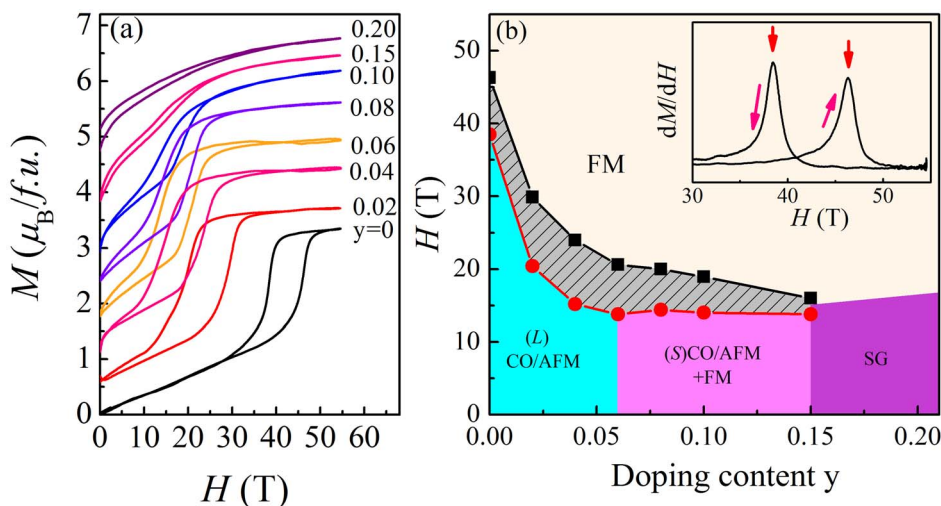


Figure 7 | (a) Magnetization as a function magnetic field measured at $T = 4.2$ K. Magnetization curves, except for the $y = 0$ data, are shifted upward for clarity. For samples $0.02 \leq y \leq 0.1$, each curve is shifted $0.6 \mu_B/f.u.$, while the curve of $y = 0.15$ is shifted $0.9 \mu_B/f.u.$ and the curve of $y = 0.2$ is shifted $1.2 \mu_B/f.u.$ (b) H - y Phase diagram, in which the solid squares and circles stand for the critical fields obtained from the up and down sweep of H , respectively. The hatched area represents the magnetic field hysteresis region accompanied by the first-order nature of the charge-order to ferromagnetic transition. The inset in (b) presents the derivative of magnetization dM/dH of sample $y = 0$, in which the critical fields of charge-order to ferromagnetic phase transition are indicated by red arrows.

spin polarization are occupied (in accordance with the 1st Hund's rule) and the hopping electron should reverse its spin, which is energetically unfavorable and thus leading to block the double exchange process²⁸. Therefore, both the AFM interaction of Cr-Mn and the empty e_g state of Cr^{3+} are proposed to be responsible for the CO suppression and FM generation in Cr^{3+} -doped $La_{0.4}Ca_{0.6}MnO_3$.

In conclusion, the phase diagrams in both T - y and H - y planes were determined through extensive magnetic measurements in $La_{0.4}Ca_{0.6}(Mn_{1-y}Cr_y)O_3$ ($0 \leq y \leq 0.2$). Upon Cr^{3+} -doping, the ground state was transformed from a robust long range CO/AFM one ($0 \leq y \leq 0.06$) to a phase separated one ($0.06 < y \leq 0.15$), and eventually to a SG-like one ($y = 0.2$). Interestingly, high magnetic field induced CO-FM phase transition was observed in samples exhibiting long range CO/AFM state or PS state, while distinct evolving paths of the critical field with y were identified as the ground state was changed. Separately, in the sample with $y = 0.2$, no CO-FM phase transition and magnetic saturation can be observed, which consisted with its SG-like state. The origin of the Cr^{3+} -doping induced CO suppression and FM generation in $La_{0.4}Ca_{0.6}MnO_3$ was discussed in terms of the antiferromagnetic coupling of Cr-Mn and local enhancement of electron hopping strength due to reduced JT effect by Cr^{3+} .

Methods

A series of samples $La_{0.4}Ca_{0.6}(Mn_{1-y}Cr_y)O_3$ ($0 \leq y \leq 0.2$) were synthesized using standard solid state reaction in air. Stoichiometric amounts of high purity La_2O_3 , $CaCO_3$, $MnCO_3$, and Cr_2O_3 were used as reagents and well ground, and the mixture was calcined at temperatures ranging from $1100^\circ C$ to $1300^\circ C$ for several times. Finally, the obtained black powder was pressed into pellets and calcined at $1400^\circ C$ for 24 hours in air. The crystalline structures of samples were investigated using X-ray diffraction with Cu $K\alpha$ radiation at room temperature. High Angle Annular Dark Field (HAADF) Scanning Transmission Electron Microscopy (STEM) and elemental mappings by using energy dispersive X-ray spectrometer (EDS) were carried out in the FEI-TITAN 80-300 microscope. Extensive measurements on the magnetic property were performed by using a Quantum Design superconducting quantum interfering device (SQUID). The measuring magnetic fields for dc and ac magnetic measurements were 100 Oe and 3.5 Oe, respectively. Electric transport measurements were performed using a standard four-probe method under various magnetic fields on a physical properties measurement system (PPMS).

Pulsed high magnetic field measurements for magnetization were performed at $T = 4.2$ K by means of a standard inductive method employing a couple of coaxial pickup coils. The pulsed magnetic field up to ~ 55 T with a duration time of ~ 50 ms was generated by using a nondestructive long-pulse magnet energized by a 1 MJ capacitor bank, which is installed at the Huazhong University of Science and Technology, China.

- Dagotto, E., Hotta, T. & Moreo, A. Colossal magnetoresistant materials: the key role of phase separation. *Phys. Rep.* **344**, 1–153 (2001).
- Tokura, Y. Critical features of colossal magnetoresistive manganites. *Rep. Prog. Phys.* **69**, 797–851 (2006).
- Hatano, T. Gate control of electronic phases in a quarter-filled manganite. *Sci. Rep.* **3**, 2904 (2013).
- Zhang, F. H. *et al.* Anisotropic-strain-induced antiferromagnetic-insulating state with strong phase instability in epitaxial films. *Appl. Phys. Lett.* **96**, 062507 (2010).
- Ding, J. F. *et al.* Dependence of negative differential resistance on electronic phase separation in unpatterned manganite films. *Appl. Phys. Lett.* **100**, 062402 (2012).
- Tokunaga, M., Miura, N., Tomioka, Y. & Tokura, Y. High-magnetic-field study of the phase transitions of $R_{1-x}Ca_xMnO_3$ ($R = Pr, Nd$). *Phys. Rev. B* **57**, 5259 (1998).
- Gorshunov, B. *et al.* Boson peak in overdoped manganites $La_{1-x}Ca_xMnO_3$. *Phys. Rev. B* **87**, 245124 (2013).
- Duc, F. *et al.* Direct evidence of magnetostructural phase transition in electron-doped manganite $Ca_{0.8}Sm_{0.16}Nd_{0.04}MnO_3$ by means of high magnetic field studies. *Phys. Rev. B* **82**, 054105 (2010).
- Xiang, P. H. *et al.* Strain-mediated phase control and electrolyte-gating of electron-doped manganites. *Adv. Mater.* **23**, 5822 (2011).
- Hatano, T. *et al.* Gate control of electronic phases in a quarter-filled manganite. *Sci. Rep.* **3**, 2904 (2013).
- Yamada, H. *et al.* Ferroelectric control of a Mott insulator. *Sci. Rep.* **3**, 2834 (2013).
- Respaud, M. *et al.* H - T magnetic phase diagrams of electron-doped $Sm_{1-x}Ca_xMnO_3$: Evidence for phase separation and metamagnetic transitions. *Phys. Rev. B* **63**, 144426 (2001).
- Li, X. G. *et al.* Jahn-Teller effect and stability of the charge-ordered state in $La_{1-x}Ca_xMnO_3$ ($0.5 \leq x \leq 0.9$) manganites. *Europhys. Lett.* **60**, 670 (2002).
- Qian, T. *et al.* Effect of Jahn-Teller interactions on the specific heat and magnetic properties of charge-ordered $La_{1-x}Ca_xMnO_3$ ($0.55 \leq x \leq 0.87$) compounds. *Phys. Rev. B* **72**, 024432 (2005).
- Lu, C. L. *et al.* Charge-order breaking and ferromagnetism in $La_{0.4}Ca_{0.6}MnO_3$ nanoparticles. *Appl. Phys. Lett.* **91**, 032502 (2007).
- Rozenberg, E. *et al.* Nanometer size effect on magnetic order in $La_{0.4}Ca_{0.6}MnO_3$: Predominant influence of doped electron localization. *Phys. Rev. B* **78**, 052405 (2008).
- Zhang, T., Wang, X. P. & Fang, Q. F. Exchange Bias Effect and Suppression of Charge Ordering Induced by a Surface Phase Separation in $La_{0.25}Ca_{0.75}MnO_3$ Nanowires. *J. Phys. Chem. C* **114**, 11796 (2010).
- Wang, Y. & Fan, H. J. The origin of different magnetic properties in nanosized $Ca_{0.82}La_{0.18}MnO_3$: Wires versus particles. *Appl. Phys. Lett.* **98**, 142502 (2011).
- Dong, S. *et al.* Surface phase separation in nanosized charge-ordered manganites. *Appl. Phys. Lett.* **90**, 082508 (2007).
- Lu, C. L. *et al.* Ru-doping-induced ferromagnetism in charge-ordered $La_{0.4}Ca_{0.6}MnO_3$. *Phys. Rev. B* **79**, 245105 (2009).
- Beaud, P. *et al.* Ultrafast structural phase transition driven by photoinduced melting of charge and orbital order. *Phys. Rev. Lett.* **103**, 155702 (2009).
- Caviezel, A. *et al.* Femtosecond dynamics of the structural transition in mixed valence manganites. *Phys. Rev. B* **86**, 174105 (2012).
- Phan, M. H. *et al.* Phase coexistence and magnetocaloric effect in $La_{5/8-y}Pr_yCa_{3/8}MnO_3$ ($y = 0.275$). *Phys. Rev. B* **81**, 094413 (2010).



24. Ouyang, Z. W., Nojiri, H. & Yoshii, S. Unusual metamagnetic transitions in $\text{Pr}_{0.5}\text{Ca}_{0.5}\text{Mn}_{0.97}\text{Ga}_{0.03}\text{O}_3$ studied by pulsed magnetic fields. *Phys. Rev B* **78**, 104404 (2008).
25. Wang, K. F. *et al.* Cluster-glass state in manganites induced by A-site cation-size disorder. *Phys. Rev. B* **73**, 134411 (2006).
26. Respaud, M. *et al.* High magnetic field study of lattice and magnetic effects on the charge-melting transition in $L_{1/2}\text{Ca}_{1/2}\text{MnO}_3$ perovskites. *Phys. Rev. B* **61**, 9014 (2000).
27. Kang, J.-S. *et al.* Resonant photoemission spectroscopy study of impurity-induced melting in Cr- and Ru-doped $\text{Nd}_{1/2}\text{A}_{1/2}\text{MnO}_3$ ($A = \text{Ca}, \text{Sr}$). *Phys. Rev. B* **68**, 012410 (2003).
28. Moritomo, Y. *et al.* Impurity-induced ferromagnetism and impurity states in $\text{Nd}_{1/2}\text{Ca}_{1/2}(\text{Mn}_{0.95}\text{M}_{0.05})\text{O}_3$. *Phys. Rev. B* **69**, 212407 (2004).
29. Martin, C. *et al.* Magnetic phase diagram of Ru-doped $\text{Sm}_{1-x}\text{Ca}_x\text{MnO}_3$ manganites: Expansion of ferromagnetism and metallicity. *Phys. Rev. B* **63**, 174402 (2001).
30. Kimura, T. *et al.* Diffuse Phase Transition and Phase Separation in Cr-Doped $\text{Nd}_{1/2}\text{Ca}_{1/2}\text{MnO}_3$: A Relaxor Ferromagnet. *Phys. Rev. Lett.* **83**, 3940 (1999).
31. Shannon, R. D. Revised effective ionic radii and systematic studies of interatomic distances in halides and chalcogenides. *Acta Crystallogr. A Cryst. Phys., Diffr., Theor. Gen. Crystallogr. A* **32**, 751-767 (1976).
32. Nair, S. & Banerjee, A. Formation of Finite Antiferromagnetic Clusters and the Effect of Electronic Phase Separation in $\text{Pr}_{0.5}\text{Ca}_{0.5}\text{Mn}_{0.975}\text{Al}_{0.025}\text{O}_3$. *Phys. Rev. Lett.* **93**, 117204 (2004).
33. Hanasaki, N. *et al.* Nature of the transition between a ferromagnetic metal and a spin-glass insulator in pyrochlore molybdates. *Phys. Rev. Lett.* **99**, 086401 (2007).
34. Lu, C. L. *et al.* Magnetic properties of Sm-based bulk metallic glasses. *J. Magn. Mater.* **322**, 2845-2850 (2010).
35. Kirkpatrick, S. Percolation and Conduction. *Rev. Mod. Phys.* **45**, 574 (1973).
36. Yun, S. H. *et al.* Giant positive magnetoresistance in ultrathin films of mixed phase manganites. *J. Appl. Phys.* **103**, 07E317 (2008).
37. Mott, N. *Conduction in Non-Crystalline Materials*. (Clarendon, Oxford, 1993).
38. Studer, F. *et al.* Magnetic moments in (Cr and Ni) doped CMR manganites as seen by soft X-ray magnetic circular dichroism. *Jpn. J. Appl. Phys., Part 1* **38**, 377-380 (1999).
39. Hu, N. *et al.* A-site disorder effects in electron-doped manganite $\text{La}_{0.4}\text{Ca}_{0.6}\text{MnO}_3$. *Appl. Phys. A* **103**, 485-491 (2011).

>

Acknowledgements

This work is supported by the National Natural Science Foundation of China (Grant Nos. 11104090, 11374112, and 11304091), the National 973 Projects of China (Grant Nos. 2011CB922101). The authors thank Dr. Neng Wan for doing the EDS. The *ac* magnetic susceptibility measurement was performed at High Magnetic Field Laboratory, Chinese Academy of Sciences, China. Thanks are due to Prof. Mingliang Tian, Ms. Xue Lou, and Mr. Langsheng Ling for this possibility.

Author contributions

C.L.L. and J.M.L. conceived and designed the experiments. M.Y., S.C.X., H.W.W., J.F.W. and Z.C.X. carried out the experiments. C.L.L., N.H. and J.M.L. wrote the paper. All the authors discussed the results and commented on the manuscript.

Additional information

Competing financial interests: The authors declare no competing financial interests.

How to cite this article: Lu, C.L. *et al.* High magnetic field phase diagram in electron-doped manganites $\text{La}_{0.4}\text{Ca}_{0.6}\text{Mn}_{1-y}\text{Cr}_y\text{O}_3$. *Sci. Rep.* **4**, 4902; DOI:10.1038/srep04902 (2014).



This work is licensed under a Creative Commons Attribution-NonCommercial-NoDerivs 3.0 Unported License. The images in this article are included in the article's Creative Commons license, unless indicated otherwise in the image credit; if the image is not included under the Creative Commons license, users will need to obtain permission from the license holder in order to reproduce the image. To view a copy of this license, visit <http://creativecommons.org/licenses/by-nc-nd/3.0/>